15. D. D. Coleman, J. B. Risatti, M. Schoell, *Geochim. Cosmochim. Acta* **45**, 1033 (1981).
16. W. S. B. Paterson, *The Physics of Glaciers* (Pergamon, New York, 1981).
17. J. Schwander and B. Stauffer, *Nature* **311**, 45 (1984).
18. D. H. Ehhalt and U. Schmidt, *Pure Appl. Geophys.* **116**, 452 (1978). The stratospheric loss was estimated by a one-dimensional diffusion model. We assume that the return flux of CH_4 from the stratosphere is negligible.
19. R. Prinn *et al.*, *Science* **238**, 945 (1987).
20. J. A. Davidson *et al.*, *J. Geophys. Res.* **92**, 2195 (1987). The experimental results fall into two distinct groups: $\alpha = 0.993$ (nine samples) and $\alpha = 0.989$ (seven samples), with no explanation of the dichotomy. We use $(\alpha - 1) \cdot 10^3 = -10$ per mil $+3/-1$ per mil.
21. The nominal value is −56.1; however, because of the nonsteady conditions of atmospheric CH_4 in 1980 (for both concentration and isotopic composition), the average $\delta(^{13}C)$ of all sources was more enriched in $^{13}CH_4$ than the value based only on the fractionation factor, and is calculated to be −55.4 per mil. Part of the difference is due to the increasing concentration: if we assume that this increase is ~1.2%/year, then the total flux in 1980 was ~9% greater than for steady-state conditions, or 50 Tg/year more than simply twice the flux of 300 years ago, for equal atmospheric lifetimes. Furthermore, the isotopic drift rate of 0.05 per mil per year (*6*) shows that the average $\delta(^{13}C)$ of the anthropogenic fluxes is more enriched than in the case of steady-state conditions. The combination of these two effects makes the mean $\delta(^{13}C)$ of the anthropogenic sources about −53.0 per mil.
22. R. J. Cicerone and J. D. Shetter, *J. Geophys. Res.* **86**, 7203 (1981).
23. H. Holzappel-Pschorn and W. Seiler, *ibid.* **91**, 11803 (1986).
24. P. J. Crutzen, I. Aselmann, W. Seiler, *Tellus* **38B**, 271 (1986).
25. H. G. Bingemer and P. J. Crutzen, *J. Geophys. Res.* **92**, 2181 (1987).
26. D. R. Hitchcock and A. E. Wechsler, "Biological cycling of atmospheric trace gases" (final report for NASA, NASA-CR-126663, 1972), pp. 117–154.
27. P. J. Crutzen, L. E. Heidt, J. P. Krasnec, W. H. Pollock, W. Seiler, *Nature* **282**, 253 (1979).
28. W. Seiler and P. J. Crutzen, *Climate Change* **2**, 207 (1980).
29. H. Craig, Y. Horibe, T. Sowers, *Science*, in press.
30. J. S. Levine *et al.*, *Nature* **318**, 254 (1985); M. A. K. Khalil and R. A. Rasmussen, *Atmos. Environ.* **19**, 397 (1985).
31. We thank K.-R. Kim and Y. Horibe for assistance in sample preparation, J. Moyers for real-time salvage, and V. Craig for making the manuscript. The dedication and skill of the Polar Ice Coring group, University of Nebraska, during the Dye 3 operation was much appreciated; they developed the drill system and did the drilling. This work was supported by NSF grants DPP82-18040, ATM82-17819, and DPP85-21486 at Scripps, and DOE contract W-31-109-Eng-38 (CO_2 Division) and NASA grant W16188 at Argonne.

11 August 1988; accepted 25 October 1988

Dynamics of a Second-Order Phase Transition: $P\bar{1}$ to $I\bar{1}$ Phase Transition in Anorthite, $CaAl_2Si_2O_8$

SUBRATA GHOSE, G. VAN TENDELOO, S. AMELINCKX

Electron microscopic study of the reversible $P\bar{1}$ to $I\bar{1}$ phase transition in anorthite (transition temperature $T_c = 516$ Kelvin) shows that the antiphase boundaries (APBs) with the displacement vector $\mathbf{R} = 1/2[111]$ become unstable at T_c, and numerous small APB loops are formed. These interfaces are highly mobile, and their vibration frequency increases strongly with temperature. These observations suggest that close to T_c, breathing-motion–type lattice vibrations of the framework cause the two different configurations around the calcium atoms, which are related by a translation of $\mathbf{R} \approx 1/2[111]$, to interchange dynamically through an intermediate $I\bar{1}$ configuration. The high-temperature $I\bar{1}$ structure is interpreted as a statistical-dynamic average of highly mobile antiphase domains of primitive anorthite.

STRUCTURAL PHASE TRANSITIONS occur when a material changes its crystallographic structure as a function of temperature and pressure. The macroscopic properties also change at the transition. Hence, the study of phase transitions is of importance for various scientific and technological applications of these materials. Whereas in first-order transitions, the symmetries of the phases above and below the transition point bear no relation to each other, the symmetries of the phases involved in a second-order phase transition are characterized by a supergroup-subgroup relation. Furthermore, second-order phase transitions are easily reversible compared to first-order transitions. Ferroelectrics as piezoelectric components and as pyroelectric detectors are some of the technologically useful materials showing second-order phase transitions. Although considerable progress has been made toward a theoretical understanding of structural phase transitions at the microscopic level (for example, concerning symmetry properties, Landau theory, and the application of static renormalization group theory to critical phenomena), our knowledge of the dynamics of the second-order phase transition is incomplete. Such a transition is associated with the formation of antiphase domains (APDs) or twins below the transition temperature, T_c. Because the interfaces separating these domains are observable by diffraction contrast in an electron microscope, the dynamics of the transition process can be studied directly. However, the only known example so far of the application of this technique is the study by Van Tendeloo *et al.* (*1*) of the α-β transition in quartz. They showed that with increasing temperature, the α_1 and α_2 twin domains break up into smaller and smaller domains close to the transition temperature, T_c (= 846 K) and that the high temperature β phase is a statistical-dynamic average of small α_1 and α_2 domains. The domain walls are mobile at and above T_c.

We have observed a similar dynamical phenomena associated with the $P\bar{1}$ to $I\bar{1}$ phase transition in anorthite (An), $CaAl_2Si_2O_8$, a framework aluminosilicate belonging to the mineral group known as feldspars. Anorthite in solid solution with albite, $NaAlSi_3O_8$, forms the plagioclase series, which are common minerals in terrestrial and lunar rocks and meteorites. Brown *et al.* discovered this phase transition, which occurs at 516 K, using high-temperature single-crystal x-ray diffraction (*2*). Their work suggested that a certain group of x-ray reflections (*c* type: $h + k =$ even, $l =$ odd; and *d* type: $h + k =$ odd, $l =$ even; where *h*, *k*, and *l* are indices of lattice planes) disappeared above T_c. Subsequent x-ray and neutron-diffraction studies have shown that the *c* reflections do not completely disappear above T_c, but persist as diffuse reflections to high temperatures close to the melting point (*3*). Refinements of the crystal structure above T_c indicated that although the framework attains virtually $I\bar{1}$ (body-centered) symmetry, the Ca atoms remain essentially in two different structural sites, mimicking their original positions in low-temperature $P\bar{1}$ (primitive) anorthite (*4*). These data suggest that the transition is not a typical displacive transformation, where the entire structure, including the Ca sites, attains $I\bar{1}$ (body-centered) symmetry above T_c; as a result, the $I\bar{1}$ structure has been interpreted as either a space average or a time average of $P\bar{1}$ anorthite. The $P\bar{1}$ anorthite is characterized by *c*-type APDs separated by antiphase boundaries (APBs). These domains have the same crystal structure but are displaced with respect to each other by a vector that is not a translation vector of the crystal structure. Electron microscopic studies have shown that the APBs with the displacement vector $\mathbf{R} = 1/2[111]$, observed in dark-field by imaging through *c* reflections, disappear above T_c but reappear on cooling in their original positions (*5*). Although some type of reorganization of the calcium sites and

---

S. Ghose, Mineral Physics Group, Department of Geological Sciences, University of Washington, Seattle, WA 98195.
G. Van Tendeloo and S. Amelinckx, University of Antwerp, Rijksuniversitair Centrum Antwerpen, Groenenborgerlaan 171, B-2020 Antwerp, Belgium.

the framework was believed to be responsible for the disappearance of the APBs, the detailed nature of the *c*-type APDs was uncertain.

We prepared samples for electron microscopy by ion-thinning 3-mm diameter discs cut from a petrographic thin section of a 1-cm thick anorthite crystal from Val di Fassa, Monzoni, Italy. Microprobe analysis indicated that the crystal is pure anorthite (An_{100}). We maintained the sample near T_c on a heating stage in the 200-kV electron microscope. We were able to control the temperature accurately above and below T_c by focusing and defocusing the electron beam. Large (~1 μm) APDs related by the displacement vector $\mathbf{R} = 1/2[111]$ were evident in dark-field images of the crystal that were made with *c* reflections (Fig. 1A). At a temperature just below T_c, the boundaries became unstable, began vibrating, and changed configuration. Simultaneously, many other APBs were created in the form of small closed loops (Fig. 1B). These boundaries were dynamic; they appeared and disappeared and changed configuration with slight changes (1 to 2 K) in temperature. When the temperature was increased about 100 to 150 K above T_c, the frequency of the APB fluctuations increased such that the individual interfaces could no longer be discerned, and the image showed a pronounced shimmering effect. On cooling through T_c, the APBs reappeared as closed loops (Fig. 1, C and D) that merged with a further decrease in temperature. The APBs always reappeared in the same original configuration after the heating and cooling cycle (Fig. 1, E and F). Presumably the APDs in the $P\bar{1}$ anorthite are pinned by defects and impurity atoms located on the domain boundaries.

On the basis of high-temperature x-ray and neutron-diffraction studies of anorthite, we constructed a model to explain the dynamical phenomena occurring near T_c (*6, 7*). The crystal structure of anorthite has four crystallographically distinct Ca positions, each located in a subcell with $c \approx 7$ Å (*c* is a crystallographic axis here). These subcells differ from each other by small deviations of atomic coordinates (~0.1 Å). Pairs of subcells related by the body-centering vector 1/2[111] have the same Si and Al distributions. Following Kempster *et al.* (*8*), we denote these positions as Ca(ooo), Ca(oio), Ca(zoo), and Ca(zio), respectively, where i and z denote translations of ~1/2[111] and ~1/2[001], respectively. The Ca atoms thus occupy cavities in the framework with similar but not identical configurations. In our model, the *c*-type APBs separate parts of the lattice that have ordered from parts that have antiordered configurations of the Ca sites. If we abbreviate the Ca(ooo) configuration by o and that of Ca(oio) by i, in one (ordered) domain, the sequence is o-i-o-i . . . , and across the boundary in the next (antiordered) domain it is i-o-i-o . . . . With increasing temperature, the framework adopts a more symmetric (body-centered) configuration as T_c is approached, mostly through the opening up of the T–O–T (T = Si or Al) angles in the aluminosilicate framework. Close to T_c, statistical fluctuations set in and breathing-motion type lattice vibrations of the framework cause the structure of the Ca sites to interchange dynamically between the configurations around Ca(ooo) and Ca(oio) [likewise Ca(zio) and Ca(zoo)] through an intermediate, symmetric ($I\bar{1}$) configuration. The configurational changes around the calcium atoms involve slight changes in the T–O–T angles only, with very little expenditure of energy. Hence, this process is easily reversible. Above T_c, large *c*-type antiphase domains will break up into small dynamically mobile domains because of rapid fluctuations of the framework. The high-temperature, body-centered phase then is a statistical-dynamic average of these small, highly mobile, $P\bar{1}$-type domains. This model is consistent with the shimmering effect observed in the electron microscope about 100 K above T_c.

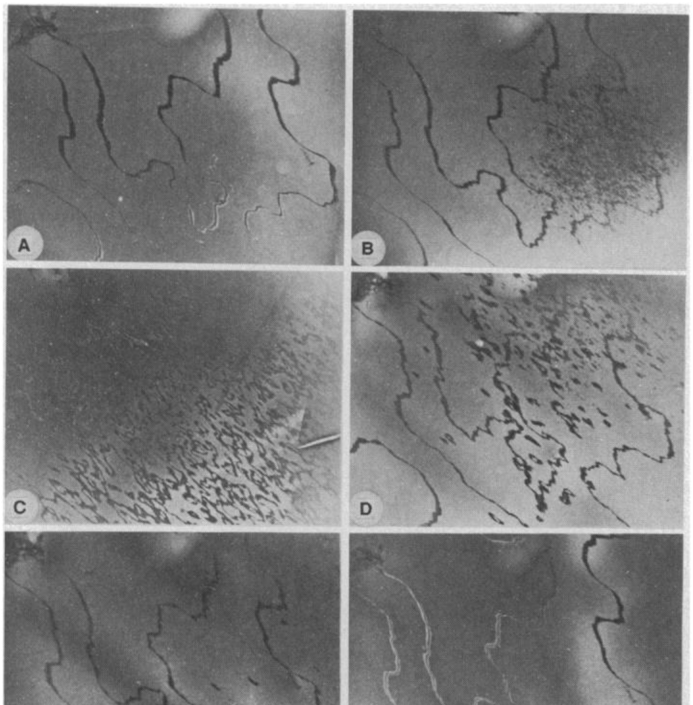

Fig. 1. Sequence of real-space (electron microscopic) images of anorthite made in the dark-field with the $(11\bar{1})$ *c*-type reflection as a function of temperature. All photographs are from the same area of the sample; (**A**) at room temperature, APBs separate large APDs; (**B**) upon heating near T_c, the APBs become mobile and many new APB loops are generated that fluctuate with a frequency that increases with temperature; (**C**) after passing through the transition and cooling again just below T_c, a large number of boundaries are observed; (**D**) these boundary loops shrink and the initial APBs begin to re-establish themselves; (**E**) at room temperature after the heating and cooling cycle; (**F**) the initial situation has been completely restored (compare with A).

The proposed transition mechanism involves a gradual approach of the aluminosilicate framework with increasing temperature to the $I\bar{1}$ symmetry as T_c is approached. Very close to T_c, an order-disorder mechanism involving the Ca atom configurations finally drives the phase transition. Hence, this transition is actually first order (nearly second order) comparable to the α-β quartz transition (*9*). However, the energies involved in the order-disorder process may be too small to be detectable in the measurements of macroscopic properties, such as unit cell dimensions and excess specific heat, which are primarily determined by the aluminosilicate framework. Hence, from the thermodynamic point of view, the transition can be treated as second order.

REFERENCES AND NOTES

1. G. Van Tendeloo, J. Van Landuyt, S. Amelinckx, *Phys. Status Solidi A* **3B**, 723 (1976).
2. W. L. Brown, W. Hoffman, F. Laves, *Naturwissenschaften* **50**, 221 (1963).
3. F. Laves, M. Czank, H. Schulz, *Schweiz. Mineral.*

Petrogr. Mitt. **50**, 519 (1970); W. Adlhart, F. Frey, H. Jagodzinski, *Acta Crystallogr. Sect. A* **36**, 450 (1980).
4. M. Czank, thesis, Eidgenoessische Technische Hochschule, Zürich (1973); S. Ghose *et al.*, *Geol. Soc. Am. Abstr. Prog.* **15**, 581 (1981).
5. W. F. Müller and H. R. Wenk, *Neues Jahrb. Mineral. Monatsh* **17** (1973); A. H. Heuer *et al.*, in *Electron Microscopy in Mineralogy*, H. R. Wenk, Ed. (Springer-Verlag, New York, 1976), pp. 345–353.
6. S. Ghose, *Eos* **66**, 1116 (1985).
7. ———, H. P. Weber, R. K. McMullan, "Physical Properties and Thermodynamic Behavior of Minerals" (Programme 24, NATO Advance Study Institute, Cambridge, England, 1987).
8. C. J. E. Kempster *et al.*, *Acta Crystallogr.* **15**, 1005 (1962); J. E. Wainwright, J. T. Starkey, *Z. Kristallogr. Mineral.* **133**, 75 (1971).
9. G. Dolino, in *Structural and Magnetic Phase Transitions in Minerals*, S. Ghose, J. M. D. Coey, E. Salje, Eds. (Springer-Verlag, New York, 1988), pp. 17–38.
10. We thank D. E. Appleman of the Smithsonian Institution, Washington, D.C., for the anorthite sample (B19995) and the National Science Foundation (grants EAR-8417767 and EAR-8719638) for support.

25 July 1988; accepted 24 October 1988

A Specific, Highly Active Malate Dehydrogenase by Redesign of a Lactate Dehydrogenase Framework

HELEN M. WILKS, KEITH W. HART, RAYMOND FEENEY,
CAMERON R. DUNN, HILARY MUIRHEAD, WILLIAM N. CHIA,
DAVID A. BARSTOW, TONY ATKINSON, ANTHONY R. CLARKE,
J. JOHN HOLBROOK

Three variations to the structure of the nicotinamide adenine dinucleotide (NAD)–dependent L-lactate dehydrogenase from *Bacillus stearothermophilus* were made to try to change the substrate specificity from lactate to malate: $\mathrm{Asp}^{197} \rightarrow \mathrm{Asn}$, $\mathrm{Thr}^{246} \rightarrow \mathrm{Gly}$, and $\mathrm{Gln}^{102} \rightarrow \mathrm{Arg}$). Each modification shifts the specificity from lactate to malate, although only the last ($\mathrm{Gln}^{102} \rightarrow \mathrm{Arg}$) provides an effective and highly specific catalyst for the new substrate. This synthetic enzyme has a ratio of catalytic rate (k_{cat}) to Michaelis constant (K_{m}) for oxaloacetate of $4.2 \times 10^6 M^{-1}\ \mathrm{s}^{-1}$, equal to that of native lactate dehydrogenase for its natural substrate, pyruvate, and a maximum velocity (250 s^{-1}), which is double that reported for a natural malate dehydrogenase from *B. stearothermophilus*.

LACTATE DEHYDROGENASE (LDH) and malate dehydrogenase (MDH) are structurally related enzymes (*1–5*) that use the same coenzyme to bring about the redox interconversion of keto- and hydroxy acids by kinetically comparable mechanisms (*6–8*) as shown in Scheme I.

Yet each enzyme is highly selective for its substrate (NAD^+, oxidized nicotinamide adenine dinucleotide; NADH, reduced NAD). For example, the MDH from *Thermus flavus* has a $k_{\mathrm{cat}}/K_{\mathrm{m}}$ value for oxaloacetate of $6.7 \times 10^6 M^{-1}\ \mathrm{s}^{-1}$ and one for pyruvate of $7.2 M^{-1}\ \mathrm{s}^{-1}$ (*9*). The LDH from *Bacillus stearothermophilus* has $k_{\mathrm{cat}}/K_{\mathrm{m}}$ values for pyruvate and oxaloacetate of 4.2×10^6 and $4 \times 10^3 M^{-1}\ \mathrm{s}^{-1}$, respectively.

In searching for the basis of this sharp discrimination between substrates there are two sources of reference. The first is comparison of gene-derived and protein-derived amino acid sequences: the primary structures of 20 LDHs and 6 MDHs are known. The second is crystallographic: there are several x-ray structures of LDH in its apo (free enzyme) (*10*), binary (enzyme-NADH) (*11*), and ternary (enzyme-NADH-substrate analog) (*12–14*) forms and a binary structure of MDH (*2, 15*).

Despite these guidelines, it was not possible to predict with conviction the elements of the proteins that select one substrate and reject the other. For example, there is no MDH structure with a bound substrate analog. A comparison of the amino acid sequences of LDH and MDH is not definitive. Despite their similarity in secondary and tertiary structure demonstrated by crystallographic studies, they show only a limited sequence identity; 19% between the LDH from *B. stearothermophilus* (*16*) and the MDH from *T. flavus* (*17*), both thermophilic prokaryotes. Even in the sections of polypeptide that we judge constitute the catalytic pocket, the identity is only 35% and any or all of the 31 amino acid changes around the active site could contribute to the difference in specificity (*18*).

```
    * *  * *  *      **       **  *   * *
MDH GAAPRKAGMER    VGNP   MT-RLDHNR   GNHSS
LDH G-ANQKPGETR    ATNP   SGTILDTAR   GEHGD
    98  -   109  138-141  163 - 171  193-197
     (no 104)

                           **   **        *
                    AQ-RGAAIIQARGAS   SAAN
                    VRDAAYQIIEKKGAT   GIAM
                    232     -   246  249-252
```

One method of testing hypotheses for substrate discrimination is to use mutagenesis to synthesize the putative new dehydrogenase structure and test its substrate specificity. This approach is not dissimilar to earlier chemical tests of catalytic mechanisms by the synthesis of a thiol proteinase from a serine proteinase (*19*). We report here successful attempts to change the specificity of *B. stearothermophilus* LDH to discriminate against pyruvate and in favor of oxaloacetate. The designs were based on a detailed understanding of the mechanism of LDH, an understanding acquired by a combination of chemical modifications, site-specific amino acid substitutions, transient and steady-state kinetic measurements, and the exploitation of optical probes (*3, 7, 20–24*). We expect the same catalytic mechanism (*6*) will prevail in the redox interconversion of oxaloacetate and malate and so make no alteration to the residues that have identifiable catalytic roles.

The spatial relation of residue 197 to the active site is shown in Fig. 1, the negative charge of the native aspartate carboxylate group is 0.8 nm from the substrate. This aspartate residue, unlike Asp^{168} (*22*), has no known catalytic function, but is always a neutral residue in MDH. If charge conservation (*24*) plays a large part in substrate discrimination, then substituting this residue for the neutral asparagine ought to select against pyruvate (charge −1) and in favor of oxaloacetate (charge −2). The steady-state catalytic properties of this modified enzyme (Table 1) broadly fulfill the prediction. There is a 32-fold reduction in catalytic efficiency against pyruvate (as measured by $k_{\mathrm{cat}}/K_{\mathrm{m}}$) and only a 1.3-fold reduction against oxaloacetate; the selectivity, therefore, shifts toward oxaloacetate (Fig.

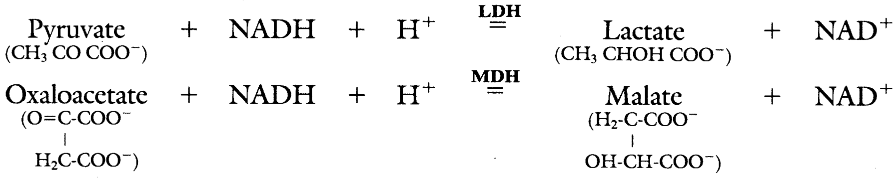

$$\underset{(\mathrm{CH_3\,CO\,COO^-})}{\text{Pyruvate}} + \text{NADH} + \mathrm{H}^+ \overset{\text{LDH}}{=} \underset{(\mathrm{CH_3\,CHOH\,COO^-})}{\text{Lactate}} + \mathrm{NAD}^+$$

$$\underset{\left(\begin{array}{l}\mathrm{O{=}C\text{-}COO^-}\\ \ \ |\\ \mathrm{H_2C\text{-}COO^-}\end{array}\right)}{\text{Oxaloacetate}} + \text{NADH} + \mathrm{H}^+ \overset{\text{MDH}}{=} \underset{\left(\begin{array}{l}\mathrm{H_2\text{-}C\text{-}COO^-}\\ \ \ |\\ \mathrm{OH\text{-}CH\text{-}COO^-}\end{array}\right)}{\text{Malate}} + \mathrm{NAD}^+$$

Scheme I

H. M. Wilks, K. W. Hart, R. Feeney, C. R. Dunn, H. Muirhead, W. N. Chia, A. R. Clarke, J. J. Holbrook, Molecular Recognition Group, Department of Biochemistry, University of Bristol, Bristol BS8 1TD, United Kingdom.
D. A. Barstow and T. Atkinson, Division of Biotechnology, Public Health Laboratory Service Centre for Applied Microbiology and Research, Porton Down, Salisbury SP4 0JG, United Kingdom.